Title
CHARACTERIZATION AND SINTERING BEHAVIOR OF BARIUM AND STRONTIUM FERRITES

Author
Reed, James S.

Publication Date
1972-03-01

Submitted to Journal of
American Ceramic Society

LBL-815
Preprint

CHARACTERIZATION AND SINTERING BEHAVIOR OF BARIUM AND STRONTIUM FERRITES

James S. Reed and Richard M. Fulrath

March 1972

AEC Contract No. W-7405-eng-48

LBL-815

DISCLAIMER

CHARACTERIZATION AND SINTERING BEHAVIOR OF BARIUM AND STRONTIUM FERRITES

James S. Reed* and Richard M. Fulrath

Inorganic Materials Research Division, Lawrence Berkeley Laboratory
and Department of Materials Science and Engineering,
College of Engineering; University of California,
Berkeley, California 94720

ABSTRACT

BaO is essentially insoluble in $BaO \cdot 6Fe_2O_3$ and the nominal compositions $BaO \cdot 5.5Fe_2O_3$ and $SrO \cdot 5.5Fe_2O_3$ employed commercially consist of the 1:6 phase and one and two minor phases, respectively. Compacts formed by mechanical pressure filtration in a magnetic field are characterized by oriented aggregates of platy particles with planar faces and planar and curved edges. The preferred growth of faces and especially larger faces with curved edges leads to fewer edge-face-edge contacts and a greater degree of collective orientation. The great anisotropy of the firing shrinkage can be explained using a model of diffusion of vacancies from pores to face boundaries.

---

* Now associate professor of ceramic engineering, State University of New York College of Ceramics at Alfred University, Alfred, New York.

This work was done under the auspices of the United States Atomic Energy Commission.

I. Introduction

Magnetoplumbite ferrites with the nominal composition $MO \cdot 6Fe_2O_3$ or $MFe_{12}O_{19}$, $M = Ba^{2+}$, Sr^{2+}, or Pb^{2+}, are important commercial permanent (hard) magnet compositions. These materials as a group now surpass soft ferrites in production volume and projected dollar growth rate.[1] Relative to their commercial importance, however, the number of technical papers on the hard ferrites is quite limited. The majority of the literature on hard ferrites is concerned with the correlation of magnetic properties with ionic composition;[2-8] the majority of the papers dealing with processing are of an empirical nature and involve relatively impure systems that have not been carefully characterized.[9-14]

Shirk and Buessem[4] have recently shown that whereas the intrinsic spontaneous magnetization of single crystals of $BaFe_{12}O_{19}$ and $SrFe_{12}O_{19}$ are practically identical, the intrinsic coercive force of $SrFe_{12}O_{19}$ is about 10% higher; both are considered superior magnetically to $PbFe_{12}O_{19}$. It is also clear that for a high magnetic energy product and coercive force, a fine crystallite size $\approx$1 μm, oriented crystallographic texture, and zero porosity are preferable microstructural features for polycrystalline materials. In practice, nonstoichiometric compositions, e.g., $BaO \cdot 5.3Fe_2O_3$-$BaO \cdot 6Fe_2O_3$, often containing inorganic additives which may enter into solid solution or form second phases, are employed. The particular role of the additives and the character of nonstoichiometric compositions have not been clearly documented. Phase equilibria have been published for the systems PbO-Fe_2O_3 in air[15] and $2BaO \cdot Fe_2O_3$-Fe_2O_3 in air[16] and as a function of the oxygen pressure.[17] For the latter system the results are somewhat at variance. Recently it has been stated by

Stuits[18] that no investigations have been reported for the sintering and grain growth kinetics of these systems and an understanding of the structure of nonstoichiometric materials is as yet unclear.

This paper presents a discussion of the characterization and sintering behavior of $BaO \cdot 6Fe_2O_3$, $BaO \cdot 5.5Fe_2O_3$, and $SrO \cdot 5.5Fe_2O_3$ at temperatures $\leq 1250°C$ and an oxygen pressure of 1 atm.

II. Experimental Procedure

(1) Material Processing

Large 2500 gram batches of $BaO \cdot 6Fe_2O_3$, $BaO \cdot 5.5Fe_2O_3$, and $SrO \cdot 5.5Fe_2O_3$ powders were compounded from reagent grade Fe_2O_3* and $BaCO_3$ or $SrCO_3$. The dry materials were carefully weighed into a low-ash rubber lined ball mill containing clean Teflon balls and isopropyl alcohol. After roll milling/mixing for 48 h, the alcohol was evaporated at 85°C and roll milling continued for 24 h.

(2) Preliminary Characterization Studies

Portions of the homogeneously mixed powders were calcined in platinum crucibles at several temperatures in the range 1000°-1350°C at 1 atm O_2, to create a series of specimens for X-ray diffraction analyses.

Also, portions of the $BaO \cdot 6Fe_2O_3$ and $BaO \cdot 5.5Fe_2O_3$ were pressed isostatically at 30,000 psi into a crucible and lid. Each crucible was filled with powder of the same composition, capped, and fired in a larger platinum crucible at 1140°C and 1 atm O_2 for 4 h. The fired crucibles and powder were then employed for continuous thermal gravimetric analyses

---

*Reagent-grade Fe_2O_3, Baker and Adamson, Allied Chemical Corp. New York, New York.

at an elevated temperature, similar to the studies by Atkin et al.:[19] In the first run, the $BaO \cdot 6Fe_2O_3$ powder was mixed with $BaCO_3$ to bring the composition to $BaO \cdot 5.5Fe_2O_3$ (after calcining), the mixture was isostatically pressed around a platinum wire, and the resulting ca. 25 gram cylindrical specimen was suspended in the $BaO \cdot 6Fe_2O_3$ crucible, contained in a hollow platinum cylinder, by means of a long platinum wire extending from the specimen through a small hole in the crucible lid and platinum cover to one arm of a recording microbalance (sensitivity ± 1 mg). The specimen was then heated at 200°C/h to 1400°C and held at this temperature for 108 h. A second run was conducted at 1250°C and 1 atm O_2 for 96 h using a specimen of $BaO \cdot 5.5Fe_2O_3$, mixed with $BaCO_3$ to bring the composition to $BaO \cdot 5Fe_2O_3$, and a crucible of composition $BaO \cdot 5.5Fe_2O_3$. A third run consisted of a specimen with the composition $BaO \cdot 6Fe_2O_3$ suspended in a crucible with a composition $BaO \cdot 5.5Fe_2O_3$ at 1315°C and 1 atm O_2 for 64 h.

Specimens from the long term thermal gravimetric analyses described above were examined using standard optical microscopy, X-ray diffraction, and electron microprobe techniques.

(3) Sintering Studies

The remaining material prepared as described in section (1) was employed for investigating the sintering behavior. All $SrO \cdot 5.5Fe_2O_3$ was calcined in air at 1075°C for 8 h; $BaO \cdot 6Fe_2O_3$ and $BaO \cdot 5.5Fe_2O_3$ were calcined in air at 1150°C for 8 h. Higher calcination temperatures yielded a product that could not be easily pulverized into a fine powder on grinding in a polyurethane lined vibratory mill using Teflon media.

Resulting powders were then wet milled/mixed for 24 h with an aqueous 3% Carbowax solution using Teflon media.

Magnetically aligned specimens were formed by mechanical pressure filtration in a magnetic field (permeable pistons of magnetically permeable iron, stainless steel die body, applied field with air gap in diameter $\geq$5000 gauss, 6000 psi). Specimens as formed were ca. 2.5 cm in diameter x 1 cm thick and of 40-45% porosity. After drying, all specimens were heated at 200°C/h to 1150°C for 10 min in 1 atm O_2, cooled, and brought to a uniform thickness by rubbing on silicon carbide paper using only finger pressure. The dimensions and weight of all specimens were subsequently measured.

All specimens were heated in 1 atm O_2 at 200°C/h in a Pt-20% Rh wound furnace and held for a specific length of time at sintering temperatures of 1150° or 1250°C. After cooling (quite rapidly to 600°C), the weight and dimensions were again measured.

After sintering, X-ray diffraction patterns were made of each planar surface and in a few cases after mechanically abrading one surface to expose interior material (Norelco X-ray diffractometer, 1° 2θ/min., Cu target, curved crystal monochromator). Also, scanning electron micrographs were taken of as fired surfaces of all specimens and electron microprobe analysis was employed to ascertain the chemical concentration of phases present in $BaO \cdot 5.5Fe_2O_3$ and $SrO \cdot 5.5Fe_2O_3$ specimens which exhibited exaggerated grain growth.

III. RESULTS AND DISCUSSION

(1) Characterization Studies

Phase equilibria for the system $2BaO \cdot Fe_2O_3$-Fe_2O_3 in air[16] shows $BaO \cdot 6Fe_2O_3$ to be congruent melting; in addition, BaO is shown to be quite soluble in $BaO \cdot 6Fe_2O_3$ to a limit of ca.$BaO \cdot 4Fe_2O_3$. Similarly, a single phase region between $PbO \cdot 4Fe_2O_3$ and $PbO \cdot 6Fe_2O_3$ has been advanced[15] for the system PbO-Fe_2O_3 in air. More recent work by Van Hook[17] conducted at controlled levels of oxygen pressure shows that BaO is essentially insoluble in $BaO \cdot 6Fe_2O_3$ and $BaO \cdot 6Fe_2O_3$ is incongruent melting at ≤ 40 atm O_2 (eutectic temperature between $BaO \cdot Fe_2O_3$-$BaO \cdot 6Fe_2O_3$ is 1315°C at 1 atm O_2). No phase diagram has been determined for the system SrO-Fe_2O_3.

All of the results obtained in this work support the findings that BaO is very nearly insoluble in $BaO \cdot 6Fe_2O_3$. In the first long-term thermal gravimetric analysis, the weight loss was $\leq 0.3\%$; in the subsequent thermogravimetric runs no weight loss was detected. The thermodynamics of phase equilibria indicate that for isothermal conditions the activity of different compositions is invariant in a two-phase field but variant in a single phase field. In the thermogravimetric experiments the anticipated mechanism for a change in weight is the vapor transport of BaO between the specimen and crucible. The constancy of weight implies that the activity of BaO is invariant and the system with the nominal composition $BaO \cdot 5.5Fe_2O_3$ is comprised of two phases.

X-ray diffraction of $BaO \cdot 6Fe_2O_3$ yielded the set of peaks indexed by ASTM for this material. Shortly after the program was underway, a curved crystal monochromator was introduced into the X-ray detection system permitting the use of a CuKα radiation source. These changes

greatly increased the intensity and resolution of the diffraction maxima. With the new diffraction set up, an additional broad low intensity peak was apparent at $\underline{d}$ = 3.16 Å for $BaO \cdot 5.5Fe_2O_3$ and $SrO \cdot 5.5Fe_2O_3$ which was not present for the 1:6 composition. This additional peak was observed to sharpen and increase in intensity for a higher calcining temperature and has subsequently been observed to correspond to the most intense diffraction maxima for a synthetic amber specimen of $BaO \cdot Fe_2O_3$.

Optical microscopy and electron microprobe analysis of the first thermal gravimetric specimen for which excessive grain growth had occurred revealed an amber non- or slightly magnetic second phase concentrated along the grain boundaries of the major phase (Figure 1). Figures 2 and 3 show the concentration profile across the grain and boundary phase that was obtained using a storage oscilloscope and 1 μm step scanning concentration analysis, respectively. These results clearly show that the concentration profile at the boundary is quite sharp and the boundary phase is $BaO \cdot Fe_2O_3$. Microprobe analyses of sintered specimens gave identical results except that some of the second phase was occluded in the grains.

Results for $SrO \cdot 5.5Fe_2O_3$ were somewhat different. X-ray diffraction patterns showed the same set of peaks as for $BaO \cdot 6Fe_2O_3$ except for some differences in the distribution of relative intensities; additional weak maxima were observed at $\underline{d}$ = 3.16 Å and $\underline{d}$ = 2.71 Å. Electron microprobe analysis of a 1250°C sintered specimen of $SrO \cdot 5.5Fe_2O_3$ exhibiting exaggerated grain growth showed inclusions ca.5μm with a higher Sr/Fe concentration (approximately $SrO \cdot Fe_2O_3$) in the major $SrO \cdot 6Fe_2O_3$ phase, and secondary elongated regions of a very high Fe/Sr phase apparently Fe_2O_3

containing a small amount of SrO in solid solution. Results from the powder preparation studies for X-ray diffraction specimens suggest that the eutectic temperature between $SrO \cdot 6Fe_2O_3$ and $SrO \cdot Fe_2O_3$ is 1180°-1280°C (vs 1315°C for the corresponding barium ferrite system) and the incongruent melting temperature for $SrO \cdot 6Fe_2O_3$ at 1 atm O_2 is definitely <1250°C and perhaps <1150°C (vs 1455°C for $BaO \cdot 6Fe_2O_3$). The extra diffraction peak at $\underline{d}$ = 3.16 Å corresponds to the 1:1 phase but that at $\underline{d}$ = 2.71 Å may correspond to either the 1:1 phase or α-Fe_2O_3.

(2) Grain Growth and Crystallite Orientation

Scanning electron micrographs of specimens of $BaO \cdot 6Fe_2O_3$ and $BaO \cdot 5.5Fe_2O_3$ heated to 1250°C for 10 min and $SrO \cdot 5.5Fe_2O_3$ heated to 1150°C for 10 min revealed particles that were platy in shape. Diameters ranged up to 1-2 μm but many faces were only a few tenths of a micron; thickness of the larger particles were typically 0.5-1 μm for the barium ferrites and 0.3-0.5 μm for the strontium ferrites. All faces were characteristically planar and many faces were nearly regular hexagons. Edges were typically planar and convex but a significant minority appeared to be rounded with both convex and concave edge curvatures. Imperfect grain alignment was obvious and arose from aggregation of particles with edge-face-edge contacts incompletely broken down on milling (Figure 4). In the systems $MO \cdot 5.5Fe_2O_3$, small rounded, poorly wetting droplets* 1/4-1/2 μm, were apparent on the faces of larger particles (Figure 5).

Further heating leads to the disappearance of submicron faces and a decrease in the proportion of edge-face-edge contacts. Growth of the

---

*It is not implied that the droplets are liquid.

faces is clearly more rapid than that of the thickness. Examination of the micrographs suggests that the larger faces with curved edges grow most rapidly creating even larger particles with convex and concave edge curvature until a pseudo-skeleton of these larger particles is formed with edge-edge contact (Figure 6). This growth character occurs especially rapidly for $BaO \cdot 6Fe_2O_3$ and can be thought of as a form of exaggerated grain growth that is encouraged by the great diffusional and shape anisotropy of the particles, preferred orientation, and edge-face-edge contact of the packing character. The rounded "droplets" on the faces grow to about 2 μm in diameter after several hundred minutes; correlation of these observations with the microprobe results, suggests quite certainly that the "droplets" are the $MO \cdot Fe_2O_3$(1:1) phase. The rate of grain growth is much greater for $BaO \cdot 6Fe_2O_3$ than for $BaO \cdot 5.5Fe_2O_3$ and the onset of the exaggerated grain growth occurs much sooner for the 1:6 composition. The presence of the 1:1 phase (and perhaps Fe_2O_3 in $SrO \cdot 5.5Fe_2O_3$) between the faces of the 1:6 phase, accordingly, plays an important role in restricting grain growth, as expected theoretically.[20] Petrographic micrographs of one specimen from the long term thermal gravimetric study revealed amber 1:1 droplets scattered across large faces (defining pores) and a continuous distribution along grain boundaries; however, this specimen had been heated at 1400°C. $SrO \cdot 5.5Fe_2O_3$ heated to 1250°C, for which a small amount of liquid apparently forms, shows extremely rapid exaggerated grain growth; this behavior in the presence of a dissolving liquid is expected theoretically.[20] In specimens of $SrO \cdot 5.5Fe_2O_3$ heated to 1150°C, the "droplets" of the 1:1 phase appear to be more prevalent

at lines of contact than for the corresponding barium ferrite specimens.

The increase in the degree of preferred orientation on sintering has been discussed briefly by Tokar[21] and is known to be connected with grain growth. In this study a crystallographic orientation parameter (q) was determined by X-ray diffraction intensity analysis of specimens positioned in the specimen holder with the exposed face representing a plane normal to the direction of the applied pressure and magnetic field on fabrication. Gillam and Smethurst[22] have discussed in detail the technique for calculating q from selected diffraction maxima. As seen in Figure 7, q increases only slightly for the major increase in density and appears to vary linearly with the differential shrinkage;* this period is characterized by the disappearance of submicron faces and only very slight growth of edge thickness. The greatest increase in q occurs as the densification rate decreases and exaggerated grain growth begins. The change in q is clearly concomitant with the particular manner of grain growth described earlier.

(3) Densification

Densification kinetics are illustrated in Figure 8. After about 100 min of elapsed time at temperature, the density increases linearly with the logarithm of time for all compositions. The initial slope of the densification curve for $SrO \cdot 5.5Fe_2O_3$ at 1150-°C is distinctly concave downwards and for $BaO \cdot 6Fe_2O_3$ the slope is initially small but then increases rapidly during the first 100 min.

---

*Difference between diametrical and height shrinkage.

The diffusivity in the 1:6 crystals can be expected to be markedly anisotropic. In $NaO \cdot 11Al_2O_3$(β-Al_2O_3), a phase closely related structurally, the diffusion of Na^+ is essentially two dimensional and is confined to the Na-containing plane normal to the c-axis.

A similar marked anisotropic diffusional character for Ba^{2+} and Sr^{2+} can be expected in the 1:6 phase. The nature of the oxygen diffusion is unknown but the diffusivity can be expected to be quite anisotropic in nature. A second important factor is the high degree of particle orientation. As a consequence, the average grain boundary area will be lower in a plane parallel to the pressing direction than for a plane normal to the pressing direction, and the average spacing between interparticle contacts will be smaller parallel to the pressing direction. Grain growth causes a further increase in the degree of particle orientation.

Coble's[23] model for the sintering of crystalline solids by the bulk diffusion of vacancies from pores to grain boundaries with a concomitant $t^{1/3}$ (t = time) grain growth dependence predicts that the density should increase linearly with log time. This predicted behavior was roughly approximated for the systems containing a second phase for which a $t^{1/3}$ grain growth dependence may be anticipated;[20] the small deviation from linearity may lie in the continually changing degree of particle orientation accompanying grain growth and the anisotropy of crystallite growth. The parameter q was 0.63 for $BaO \cdot 5.5Fe_2O_3$ and $SrO \cdot 5.5Fe_2O_3$ as formed, and the value of q increased slightly more rapidly with densification (Figure 7) for $SrO \cdot 5.5Fe_2O_3$. As seen in Figure 9, q appears to vary in a linear way with differential shrinkage for the major range of densification.

The firing shrinkage is about 2 times greater in a direction normal to the preferred alignment of faces. In Figure 10, the differential shrinkage increased linearly with density and the rate and total differential shrinkage attained was higher for $SrO \cdot 5.5Fe_2O_3$ (15% vs 7% at 1150°C) than for $BaO \cdot 5.5Fe_2O_3$. Since the size of the grain faces and initial q were very nearly identical, the greater anisotropy of the firing shrinkage for $SrO \cdot 5.5Fe_2O_3$ must be associated with an inherently greater degree of anisotropic diffusion and pore elimination processes on sintering. For $SrO \cdot 5.5Fe_2O_3$ the thickness of the grains was ca.1/2 that for $BaO \cdot 5.5Fe_2O_3$. Accordingly, the spacing between face boundaries would definitely be lower for $SrO \cdot 5.5Fe_2O_3$. For a model of vacancies preferentially diffusing from pores to boundaries between faces, the greater shrinkage normal to the faces and the greater differential shrinkage for $SrO \cdot 5.5Fe_2O_3$ is quite rational. The increasing degree of shrinkage anistropy with increasing q is to be expected.

IV. Summary

$BaO \cdot 6Fe_2O_3$ cannot incorporate a significant amount of BaO and exist as a single phase. After sintering at temperatures of 1250° and 1150°C and 1 atm O_2, the nominal composition BaO $5.5Fe_2O_3$ consists of $BaO \cdot 6Fe_2O_3$ and $BaO \cdot Fe_2O_3$ and the nominal composition $SrO \cdot 5.5Fe_2O_3$ consists of $SrO \cdot 6Fe_2O_3$ and two secondary phases approximately Fe_2O_3 and $SrO \cdot Fe_2O_3$.

Compacts formed by mechanical pressure filtration in a magnetic field were characterized by small aggregates of platy particles with planar faces but both planar and curved edges. The preferential growth of faces was clearly apparent and led to a lower number of edge-face-edge contacts and an increased degree of particle orientation. Scanning

electron photomicrographs suggested that larger faces with curved edges have the highest growth rate.

The presence of the 1:1 phase markedly restricts grain growth and distinctly contrasts the initial and intermediate sintering behavior of $BaO \cdot 5.5Fe_2O_3$ from that for $BaO \cdot 6Fe_2O_3$. At 1150°C and 1 atm O_2, $SrO \cdot 5.5Fe_2O_3$ sinters more rapidly than $BaO \cdot 5.5Fe_2O_3$, exhibits a slower rate of grain growth, and a higher degree of differential firing shrinkage. At 1250°C and 1 atm O_2, all systems exhibited exaggerated grain growth. The shrinkage anisotropy can be explained using a model of vacancies diffusing preferentially to face boundaries. The higher shrinkage anisotropy for $SrO \cdot 5.5Fe_2O_3$ having a greater face diameter/thickness ratio and the increasing anisotropy of shrinkage with increasing grain orientation can, accordingly, arise from a shorter average spacing between faces in the direction of greatest shrinkage.

References

1. F. G. Brockman, "Magnetic Ceramics - A Review and Status Report," Bull. Am. Ceram. Soc., 47 [2] 186-94 (1968).

2. J. Smit and H. P. J. Wijn, Ferrites, J. Wiley and Sons, New York, 1959.

3. G. Winkler, "Eigenschaften und Aniuendungen hexagonaler Ferrite," Z. angew. Phys., 21 [4] 282-6 (1966).

4. B. T. Shirk and W. R. Buesseum, "Temperature Dependence of M_S and K_1 of $BaFe_{12}O_{19}$ and $SrFe_{12}O_{19}$ Single Crystals," J. Appl. Phys., 40 [3] 1294-6 (1969).

5. R. O. Savage and A. Tauber, "Growth and Properties of Single Crystals of Hexagonal Ferrites," J. Am. Ceram. Soc., 47 [1] 13-18 (1964).

6. B. T. Shirk and W. R. Buesseum, "Magnetic Properties of Barium Ferrite Formed by Crystallization of a Glass," J. Am. Ceram. Soc., 53 [4] 192-6 (1970).

7. A. Aharoni and M. Schieber, "Magnetic Moment of Lanthanum Magnetoplumbite Ferrite," Phys. Rev., 123 [3] 807-9 (1961).

8. M. Robbins, S. Lerner and E. Banks, "Some Effects of Charge Compensating Ions on Cation Sites Preferences in Complex Oxides," J. Phys. Chem. Solids," 24 [6] 759-69 (1963).

9. A. Cochardt, "Modified Strontium Ferrite, A New Permanent Magnet Materials," J. Appl. Phys., 34 [4] 1273-4 (1963).

10. A. Cochardt, "Recent Ferrite Magnet Developments," ibid, 37 [3] 1112-15 (1966).

11. M. Tokar, "Microstructure and Magnetic Properties of Lead Ferrite," J. Am. Ceram Soc., 52 [6] 302-6 (1969).

12. H. B. Ries, "The Technology of the Ferrites," Interceram., 1, 85-92 (1966).

13. K. Friess, "Neue Ergebnisse an Strontiumferrite-Magneten," Z. angew. Phys., 21, 90-92 (1966).

14. Siemens and A. G. Halske, Belgian Patent 687,058, March 20, 1967.

15. A. J. Mountvala and S. F. Ravitz, "Phase Relations and Structures in the System PbO-Fe_2O_3," J. Am. Ceram. Soc., 45 [6] 205-8 (1962).

16. Y. Goto and T. Tokada, "Phase Diagram of the System BaO-Fe_2O_3," J. Am. Ceram. Soc., 43 [3] 150-3 (1960).

17. H. J. VanHook, "Thermal Stability of Barium Ferrite ($BaFe_{12}O_{19}$)," J. Am. Ceram. Soc., 47 [11] 579-81 (1964).

18. A. L. Stuits, p. 447 in Ceramic Microstructures, ed. J. Pask and R. Fulrath, J. Wiley & Sons, Inc., New York, N.Y. 1968.

19. R. B. Atkin, R. L. Holman, and R. M. Fulrath, "Substitution of Bi and Nb Ions in Lead Zirconate-Titanate," J. Am. Ceram. Soc., 54 [2] 113-15 (1971).

20. M. Hillert, "On the Theory of Normal and Abnormal Grain Growth," Acta Metallurgica, 13 [3] 227-38 (1965).

21. M. Tokar, "Increase in Preferred Orientation in Lead Ferrite by Firing," J. Am. Ceram. Soc., 51 [10] 601-2 (1968).

22. E. Gillam and E. Smethurst, "Orientation Texture and Magnetic Properties of Polycrystalline Baxium Hexaferrite," Proc. Brit. Ceram. Soc., 2, 129-37 (1964).

23. R. L. Coble, "Sintering Crystalline Oxides: I," J. Appl. Phys., 32 [5] 787-92 (1961).

Figure Captions

Figure 1. Photomicrograph of specimen of $BaO \cdot 5.5Fe_2O_3$ from long-term TGA studies showing a second phase distributed along grain boundaries and surface of pores. Each grid is 45 μm on a side.

Figure 2. Photomicrograph showing BaLα emission from grain boundary and neighboring grains of a specimen of $BaO \cdot 5.5Fe_2O_3$.

Figure 3. Concentration profile obtained on electron probe step scanning across the boundary illustrated in Figure 2.

Figure 4. Scanning electron photomicrograph of $BaO \cdot 6Fe_2O_3$ compact heated 10 minutes at 1250°C (note aggregates with face/edge/face contact).

Figure 5. Photomicrograph of $SrO \cdot 5.5Fe_2O_3$ heated 135 minutes at 1150°C (note droplets on faces and between faces at top center).

Figure 6. Photomicrograph showing grains with large curved faces in $SrO \cdot 5.5Fe_2O_3$ heated 700 minutes at 1150°C.

Figure 7. The variation of orientation parameter with density.

Figure 8. Densification kinetics of $BaO \cdot 6Fe_2O_3$, $BaO \cdot 5.5Fe_2O_3$, and $SrO \cdot 5.5Fe_2O_3$.

Figure 9. The variation of orientation parameter with differential shrinkage.

Figure 10. Differential shrinkage as a function of density.

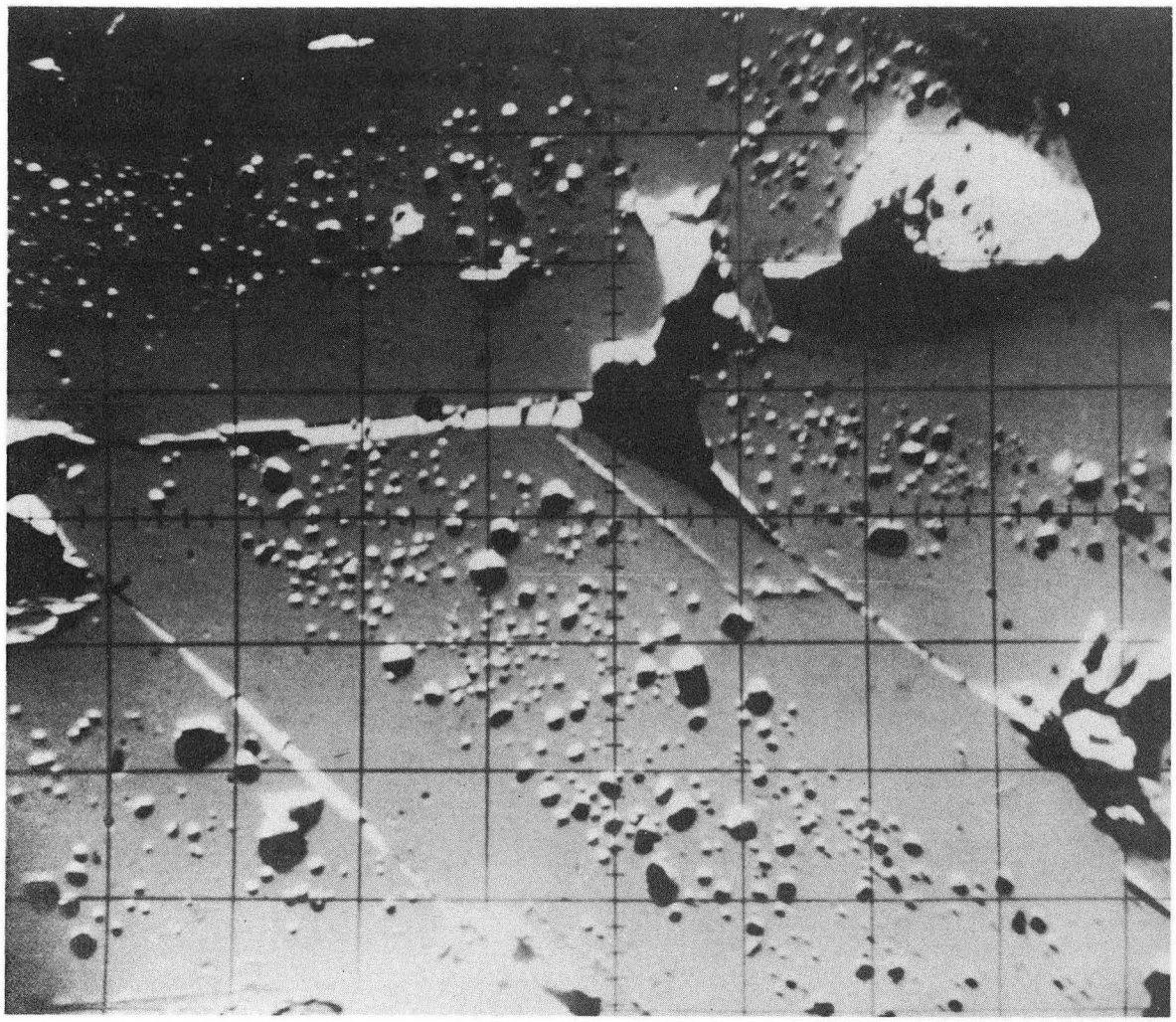

XBB 724-1951

Fig. 1

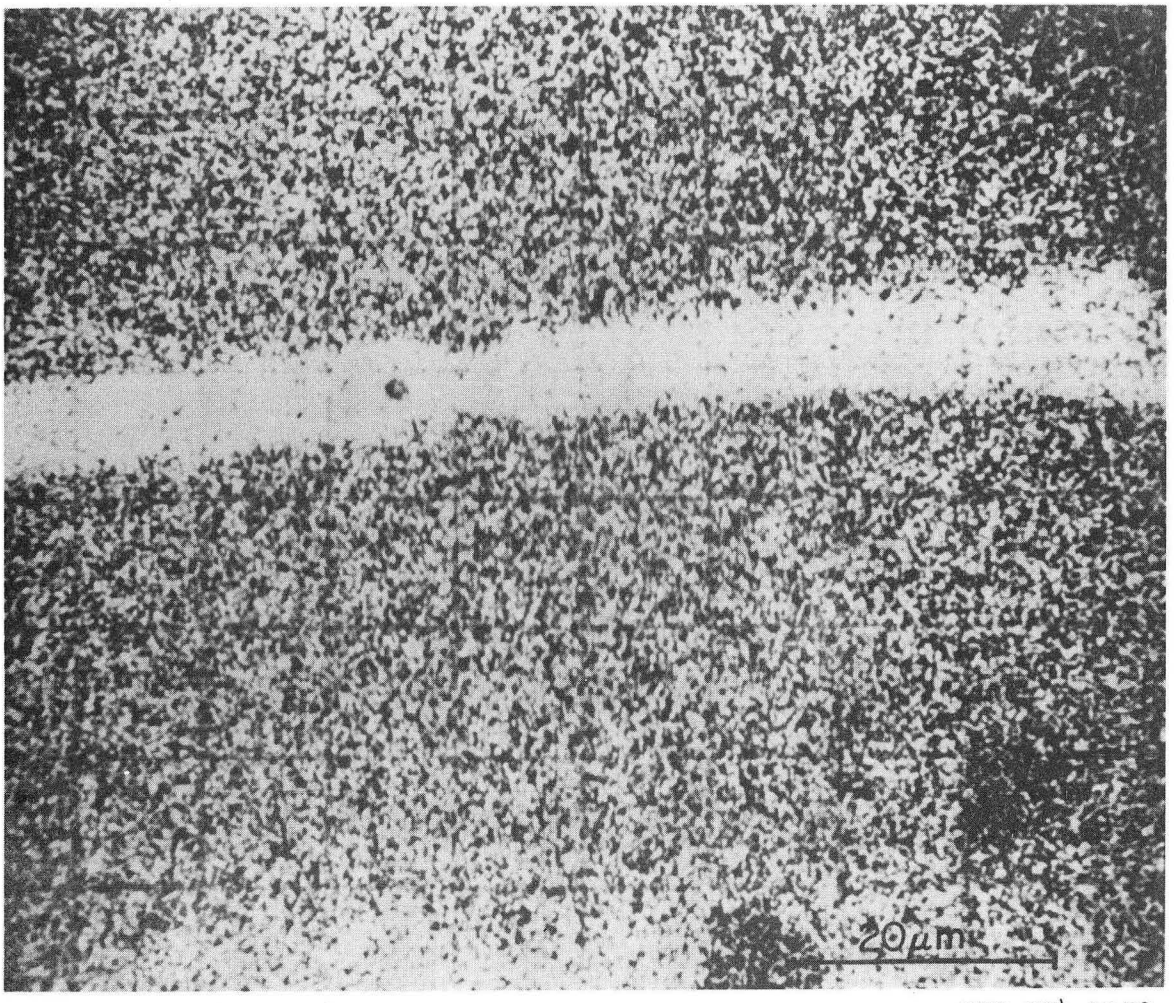

XBB 724-1953

Fig. 2

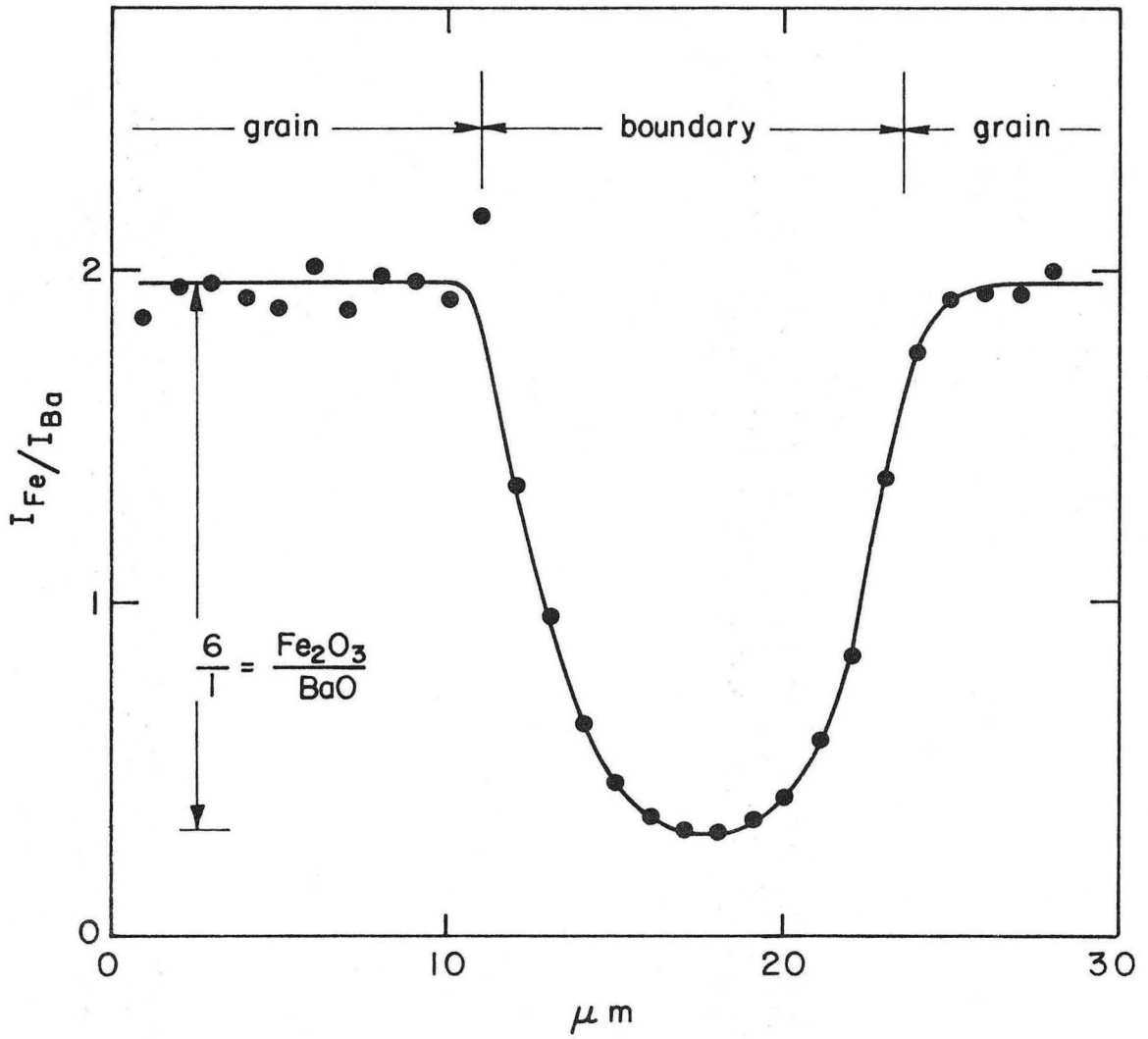

XBL723-6095

Fig. 3

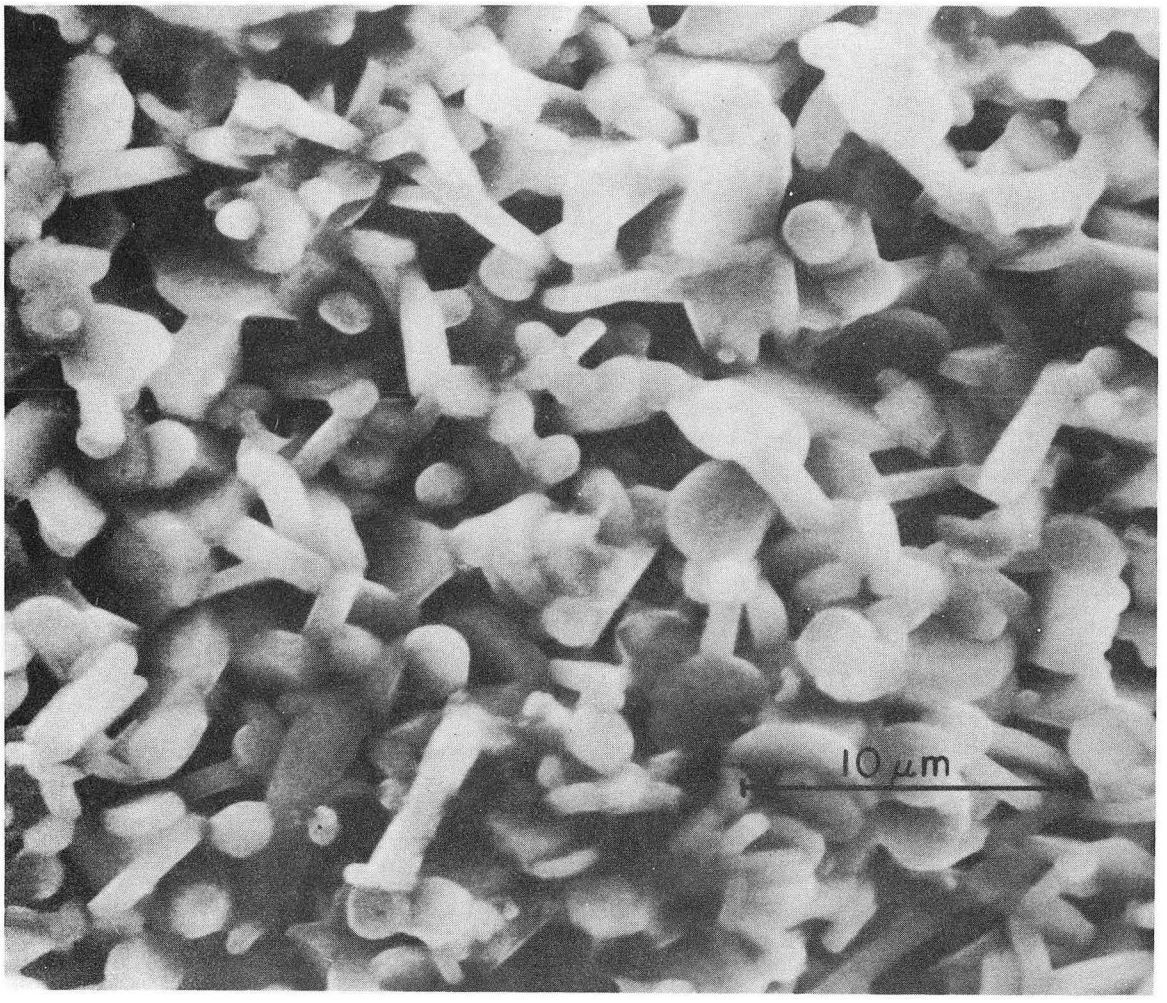

XBB 724-1954

Fig. 4

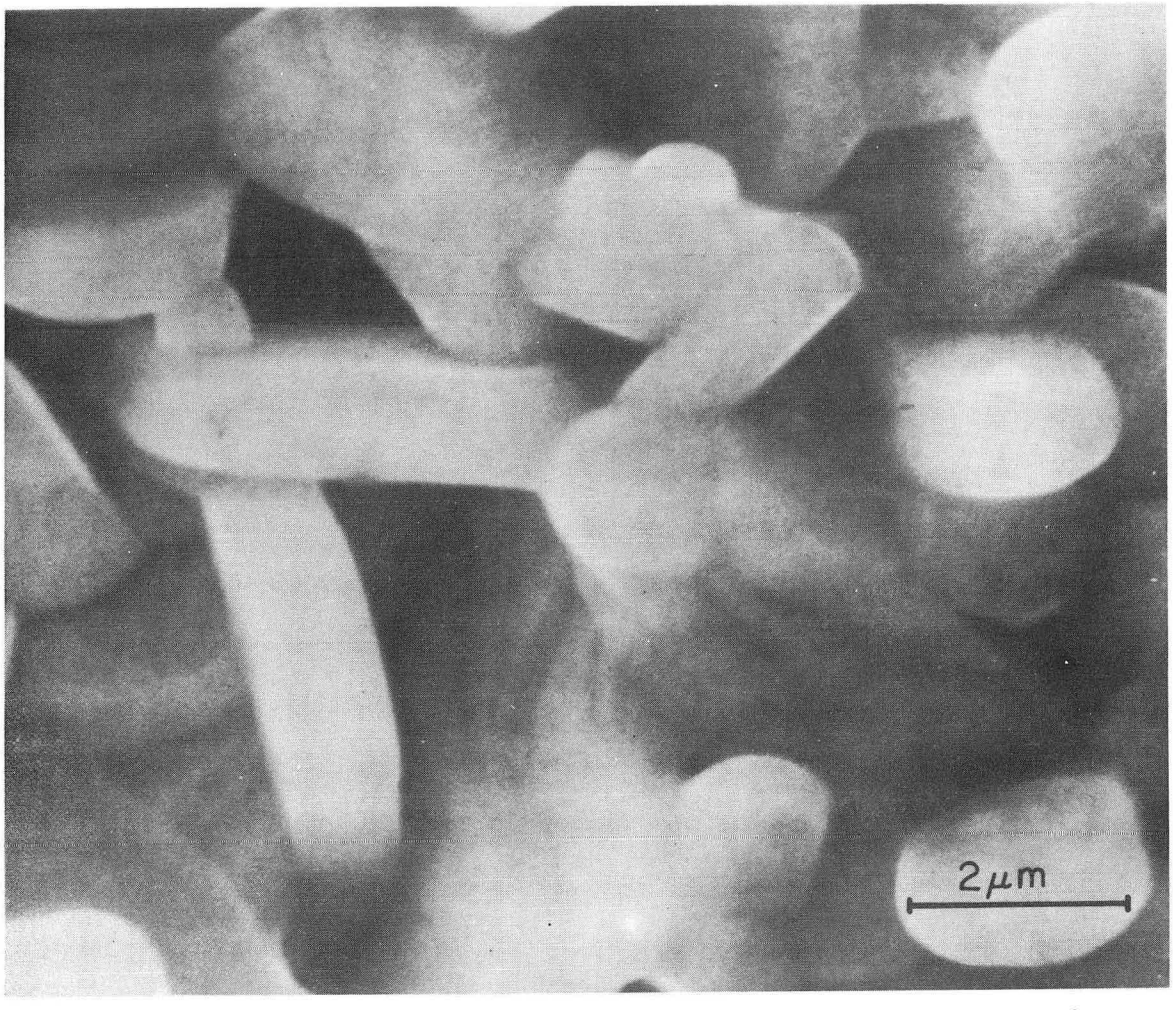

XBB 724-1950

Fig. 5

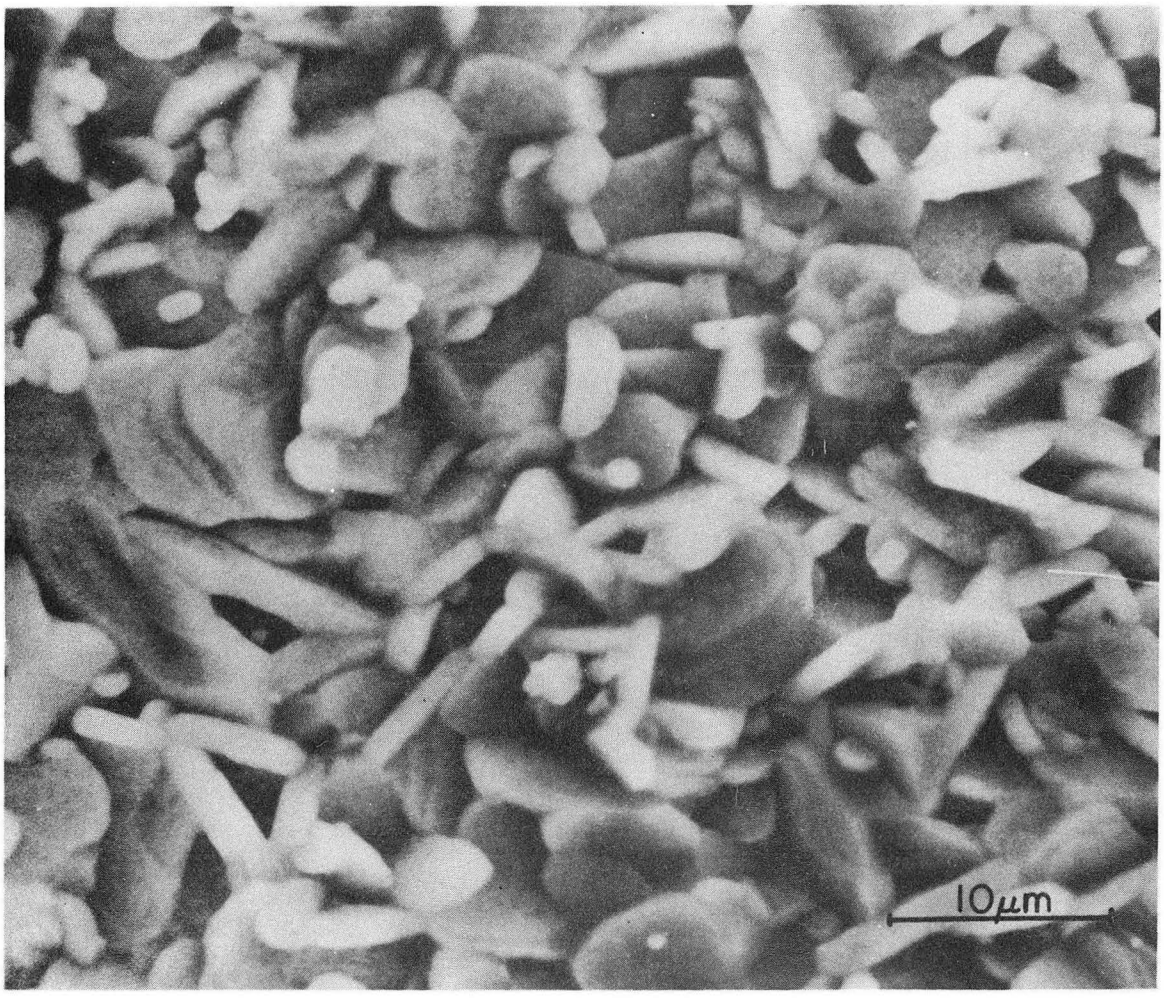

XBB 724-1952

Fig. 6

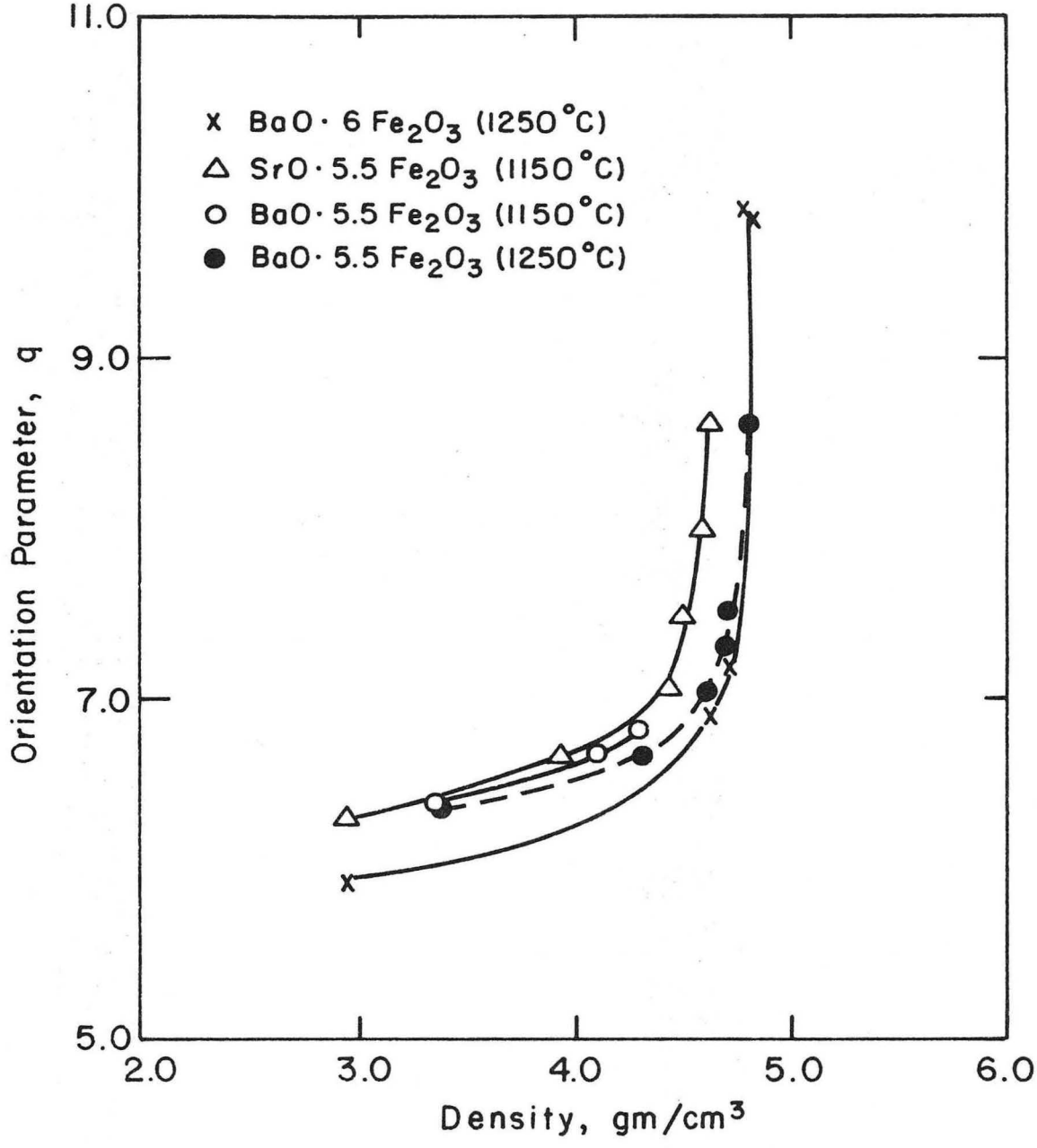
11.0
9.0
7.0
5.0
2.0
3.0
4.0
5.0
6.0
Orientation Parameter, q
Density, gm/cm³
x BaO · 6 Fe₂O₃ (1250°C)
△ SrO · 5.5 Fe₂O₃ (1150°C)
○ BaO · 5.5 Fe₂O₃ (1150°C)
● BaO · 5.5 Fe₂O₃ (1250°C)
XBL 723-6096

Fig. 7

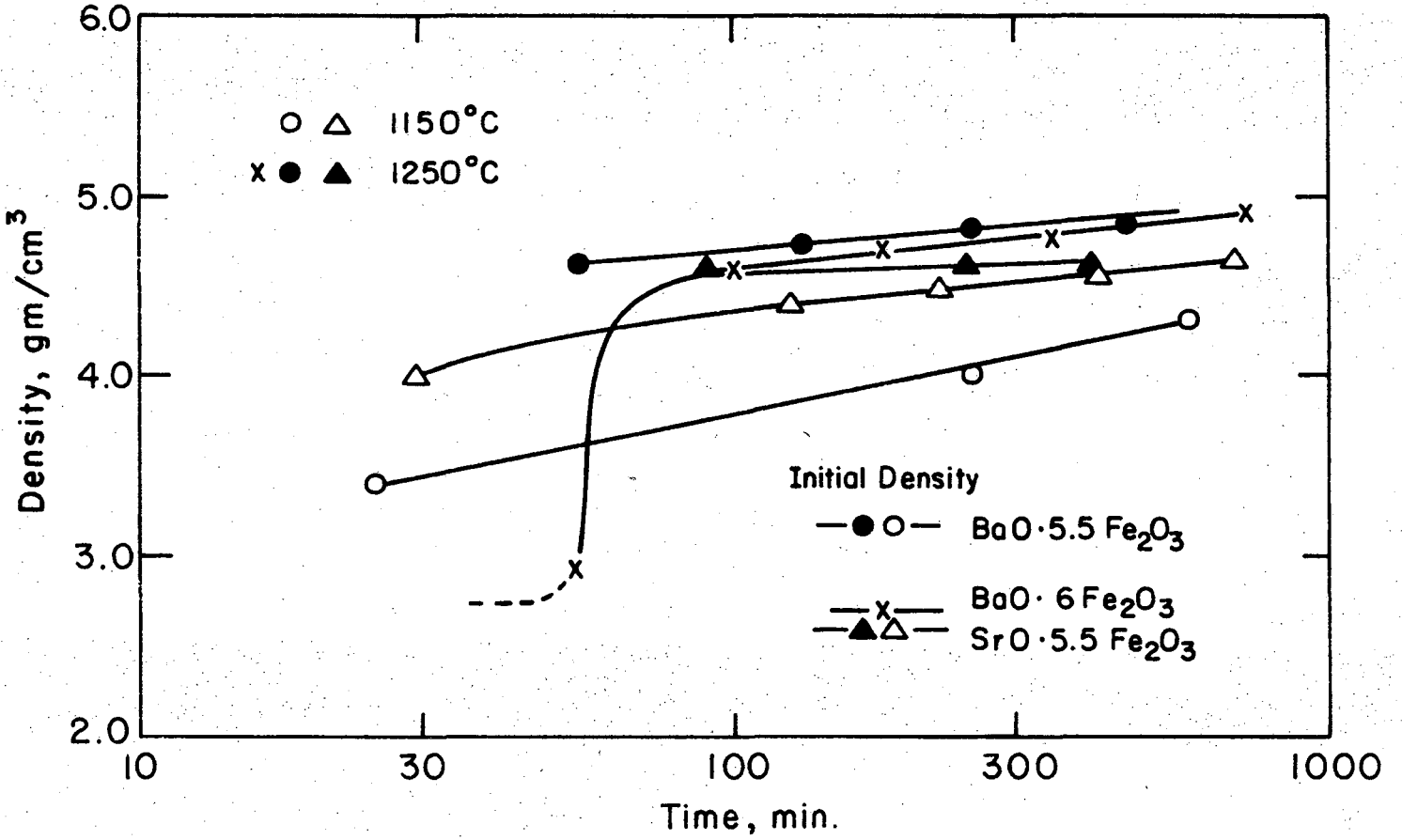

XBL 723-6097

Fig. 8

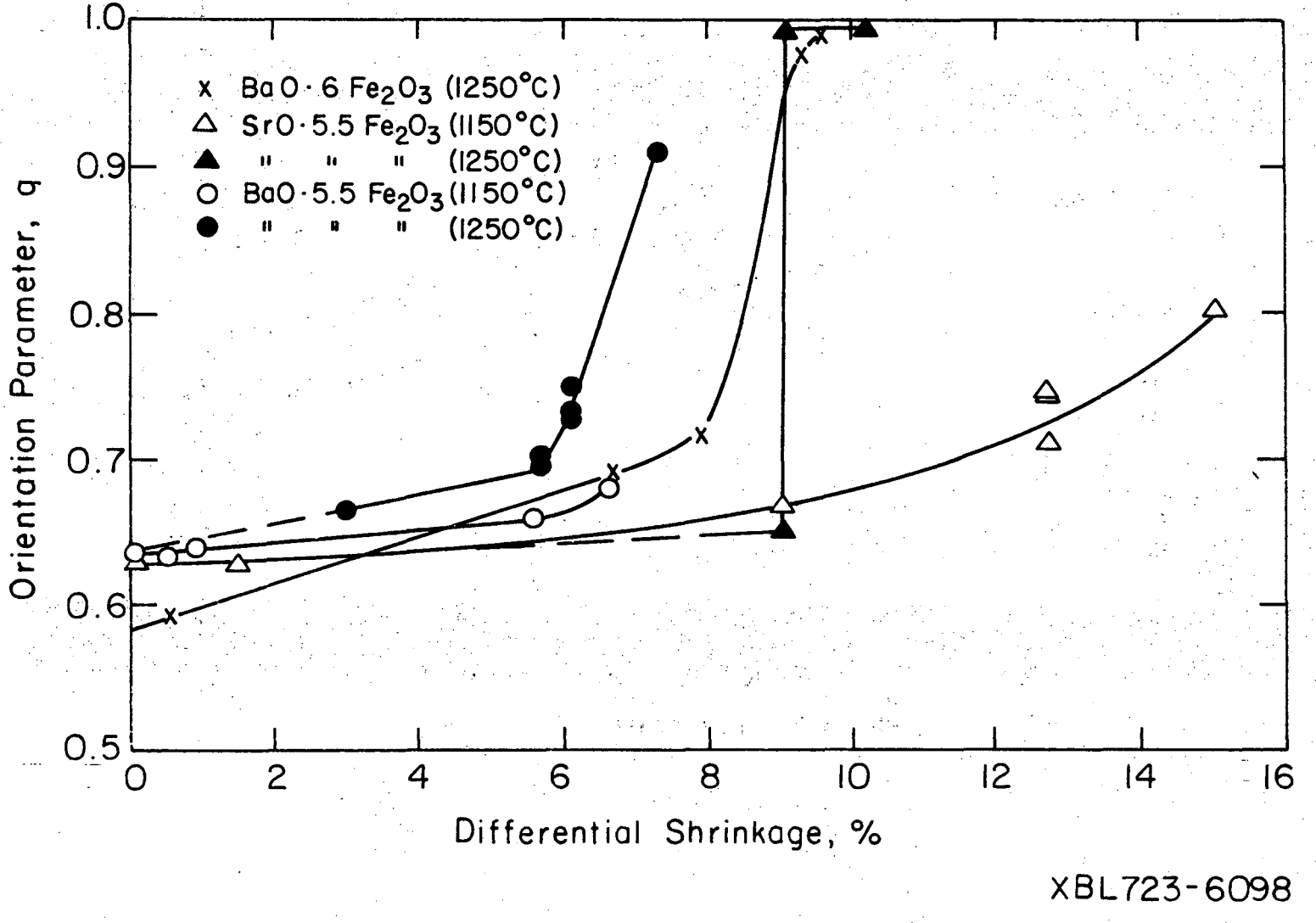

XBL723-6098

Fig. 9

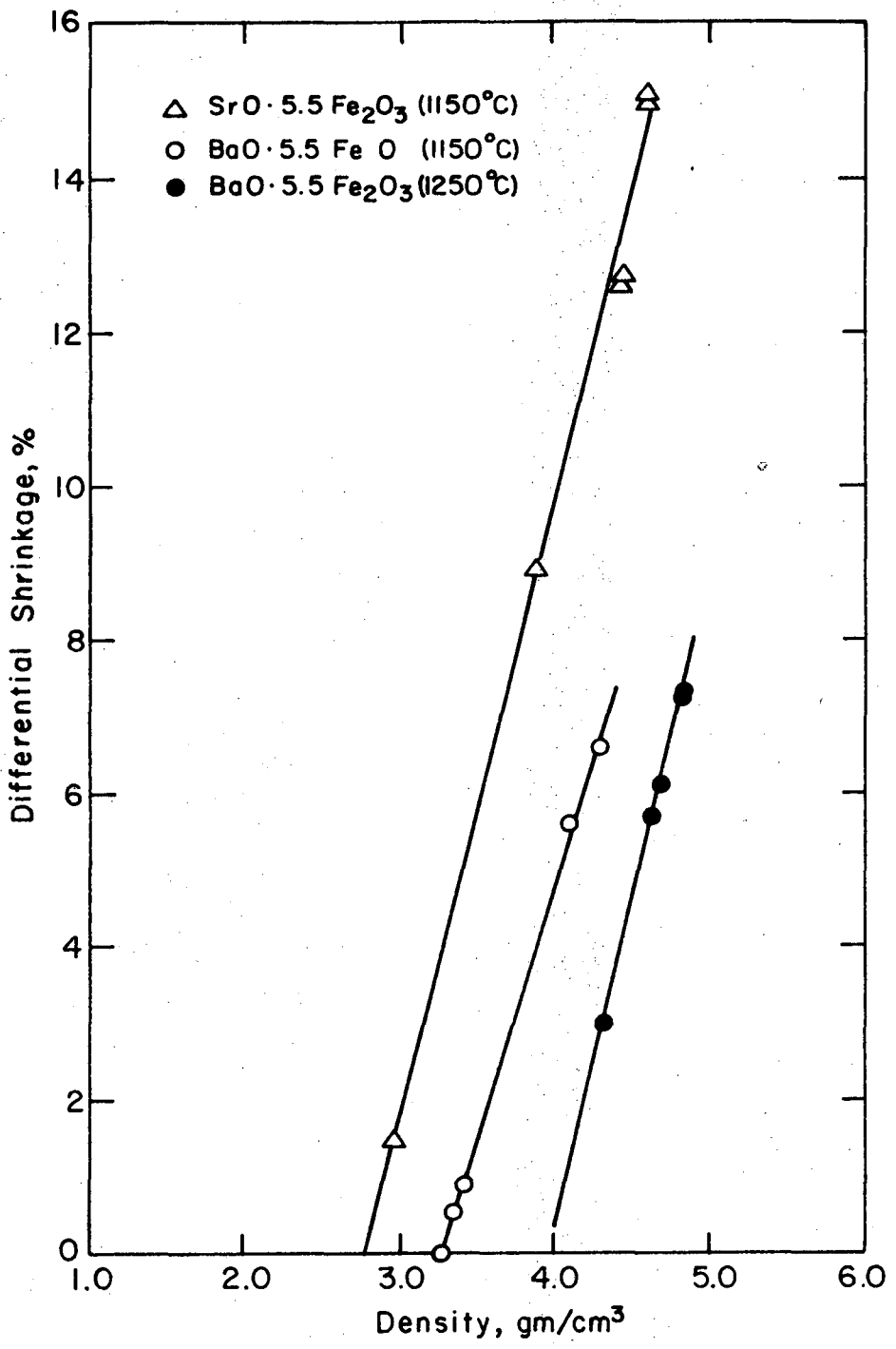

XBL723-6099

Fig. 10

TECHNICAL INFORMATION DIVISION
LAWRENCE BERKELEY LABORATORY
UNIVERSITY OF CALIFORNIA
BERKELEY, CALIFORNIA 94720